



Semnan University



Analysis of the Effect of Periodic Magnetic Field, Heat Absorption/Generation and Aspect Ratio of the Enclosure on Non-Newtonian Natural Convection

Mohammad Nemati ^a, Mohammad Sefid ^{*a}, Ahmad Reza Rahmati ^b

^a Department of Mechanical Engineering, Yazd University, Yazd, Iran

^b Department of Mechanical Engineering, University of Kashan, Iran.

PAPER INFO

Paper history:

Received: 2020-12-27

Revised: 2021-06-16

Accepted: 2021-08-18

Keywords:

Heat absorption/generation;

Lattice Boltzmann method;

Natural convection heat transfer;

Non-Newtonian fluid;

Periodic magnetic field;

Variable aspect ratio.

ABSTRACT

In the present study, natural convection heat transfer of non-Newtonian power-law fluid inside a two-dimensional enclosure with variable aspect ratio with heat absorption/generation is investigated by using the lattice Boltzmann method (LBM). The magnetic field is applied to the enclosure in uniform and periodic forms. The vertical wall and curved walls of the enclosure are at constant hot and cold temperature, respectively. The present work is validated with previous studies and the accuracy of the results is ensured. The effect of the Hartmann number, non-Newtonian power-law index, heat absorption/generation coefficient, aspect ratio and the type of magnetic field applied on the nature of flow and heat transfer are studied. The results show that increasing the non-Newtonian power-law index, Hartmann number and the heat absorption/generation coefficient reduce the Nusselt number. By increasing the heat generation/absorption coefficient, aspect ratio and decreasing the non-Newtonian power index, the effect of the magnetic field increases. Applying a magnetic field periodically compared to a uniform form leads to an increase of in Nusselt number and flow strength that this effect is greatest for shear thinning fluid and negligible for shear thickening fluid. Increase of Hartmann number and heat absorption/generation coefficient simultaneous leads to further decrease of average Nusselt number. This study could pave the way for the optimal design of industrial thermal equipment.

DOI: 10.22075/JHMTR.2021.22119.1322

© 2021 Published by Semnan University Press. All rights reserved.

1. Introduction

In recent decades, extensive efforts have been made to build high-efficiency heat exchange equipment in order to save on the consumption of raw materials and energy, as well as for environmental and economic issues [1]. The main goal is to reduce the size of the equipment for a given thermal load and increase the heat exchange capacity. If

the principles of heat transfer methods and the design of high-level heat transfer devices are well known, it will be possible to increase energy savings and reduce environmental pollution [2, 3]. Natural convection is one of the mechanisms of heat transfer and occurs when a volumetric force is applied to it by creating a density difference due to the temperature gradient in the fluid [4].

* Corresponding Author: Mohammad Sefid, Department of Mechanical Engineering, Yazd University, Yazd, Iran

The increasing growth of heat transfer study under the influence of the magnetic field inside closed enclosures has received much attention due to its high application. The characteristic of all these researched is that the fluid experiences the Lorentz force. This force affects the buoyancy flow field and heat transfer [5-7]. Among the Applications of this type of issue that magnetic field is applied, can be mention casting, metallurgy and cooling industries of electronic equipment that are installed horizontally and vertically on the walls of the enclosure containing electronic circuits, and the cavity may be located at different angles to the earth's surface [8]. The passage of electric current through a circuit and the corresponding parts produces a magnetic field. The generated magnetic field affects the current field and heat transfer. Numerous studies in this field have been done numerically, laboratory and analytical [9-11]. Ma et al. [12] examined the MHD natural convection of nanofluid in a U-shaped enclosure and showed that decreasing the velocity due to increasing the Hartmann number leads to decrease average Nusselt number, especially near the walls.

Heat generation/absorption plays a very important role in various phenomena such as nuclear energy and combustion modeling. One of the methods used by researchers to enhance the thermal performance of energy systems is the influence of a magnetic field by heat generation/absorption [13]. These studies include the study of Jami et al. [14], Maleki et al. [15] and Selimefendigil and Oztop [16]. Mliki et al. [17] investigated the natural convection heat transfer under the influence of a magnetic field inside a square cavity with a wall with a linear temperature distribution and heat generation/absorption. The results showed that increasing the strength of the magnetic field reduces the heat transfer and velocity rate and the changes in heat generation/absorption coefficient has a noticeable effect on flow characteristics and heat transfers Increasing the heat absorption /generation coefficient increases the maximum value of the stream function.

Advances in technology and the need to install electronic components in confined spaces have made the issue of natural convection heat transfer in formable (non-square) enclosures important and necessary [18]. In most recent studies, square and rectangular cavities have become more common for a variety of reasons, including the simplicity of the computational field. Shaped enclosures are used in microchannels, the casting industry, and the placement of an electronic component in unwanted spaces [19]. Formed cavities are used in microchannels, the casting industry, and the placement of an electronic component in unwanted spaces [20-22].

Most studies on heat transfer within cavities with different geometries have been based on Newtonian fluid and the effect of different parameters on the behavior of non-Newtonian fluid has not been studied much. Most of the fluid behavior used in the mechanical and chemical industries is non-Newtonian. Non-Newtonian fluid flows

have been used in many natural and industrial applications, including the transmission lines of industrial products, polymer processes, and many biological applications, such as blood flow in the body [23-25]. Unlike non-Newtonian fluids, Newtonian fluids do not have viscosity changes with pressure changes. Viscosity in a Newtonian fluid depends only on temperature and pressure and does not depend on the force applied to it. But in non-Newtonian fluids, the amount of fluid viscosity depends on the force applied to that fluid. For Newtonian fluids, the relationship between shear stress and strain rate is linear, but in non-Newtonian fluids, this relationship is nonlinear, and in this type of fluid, the time of applied of stress is effective on the amount of stress obtained. [26, 27]. Raisi [28] investigated the effect of a pair of barriers on natural convection of non-Newtonian fluid in a square cavity and concluded that as the non-Newtonian fluid power index decreases, the apparent viscosity increases and consequently the convection effects increase within the cavity. Aghakhani et al. [29] researched the MHD natural convection non-Newtonian fluid with the power-law model inside the C-shaped cavity with a ratio of different dimensions. The results of their study showed that increasing the strength of the magnetic field, aspect ratio of the cavity and the power index lead to a reduction in the effects of natural convection and heat transfer.

In the last decade, lattice Boltzmann method has grown significantly in fluid flow analysis and computational fluid dynamics. The advantage of this method compared to other conventional methods is the ease of application of boundary conditions, simpler calculations and parallelism, which is widely used to solve problems with complex geometry [30-32]. Zhang et al. [33] studied the MHD natural convection heat transfer and entropy generation of non-Newtonian fluid by LBM in the L-shaped cavity. The results stated that increasing the Hartmann number and the non-Newtonian power index lead to a decrease in heat transfer rate.

By reading previous articles, it can be seen that most researched have been about the effect of uniform magnetic field on convection flows and few studies have been done on the effect of periodic magnetic field on fluid flows. Mehryan et al. [34] analyzed heat transfer and entropy generation in a square cavity in the presence of a periodic magnetic field. The results showed that whenever a periodic magnetic field is applied, the heat transfer and flow strength are higher compared to uniform applied. Izadi et al. [35] numerically investigated the natural convection of nanofluid inside a porous square cavity under the influence of a periodic magnetic field. The results showed that the angle of applied of the periodic magnetic field has a significant effect on the rate of heat transfer and flow field.

Based on previous studies, it has been observed that so far, no studies have been conducted on the present subject, the simultaneous use of non-Newtonian fluid with power law model, heat absorption/generation and periodic magnetic field especially in this geometry with lattice

Boltzmann method. In the present work, two distribution functions are used to solve the flow field and temperature. The results are compared with previous studies. The results are presented in the form of contours, tables and graphs. In the present work, the effect of parameters affecting the nature of flow and heat transfer is investigated.

2. Definition of considered model

The geometry of problem, which is a two-dimensional enclosure containing non-Newtonian fluid, is shown in Figure 1. The magnetic field is applied both uniform and non-uniform forms from left to right and perpendicular to gravity. The curved wall of the enclosure has a cold temperature and is considered according to Equation (1).

$$x = \frac{D}{2} \left(1 - \cos \frac{2\pi y}{H} \right) \tag{1}$$

The vertical wall of the enclosure is at a hot temperature. The aspect ratio of the enclosure is defined as: AR=DH.

In this enclosure there is uniform heat absorption/generation to the power of Q. The term used to describe the magnetic field is given in equation (2), in which Bo is the amplitude and κ is the number of oscillating waves.

$$B = \frac{B_o}{2} \left(1 - \cos \frac{2\kappa\pi y}{H} \right) \tag{2}$$

The effect of parameters such as non-Newtonian fluid power index (0.8, 1 and 1.2), Hartmann number (0, 30, 60), heat absorption/generation coefficient (-10, 0 and +10), aspect ratio of the enclosure (0.5, 1, and 1.5) and the type of applied magnetic field (uniform and periodic) on the flow and heat transfer within this especially geometry is the main cause of the present study. In the present work, the Rayleigh number is 105. All borders are impenetrable and there is no slip on the surfaces. The studied flow is laminar, non-Newtonian, two-dimensional, steady and incompressible, using the Boussinesq approximation. The heat transfer of radiation, loss of viscosity and heat transfer due to the presence of a magnetic field are neglected [14]. Due to the fact that in real and industrial applications, fluids with high Prandtl number are used, in the present work, Prandtl number 100 is considered [29].

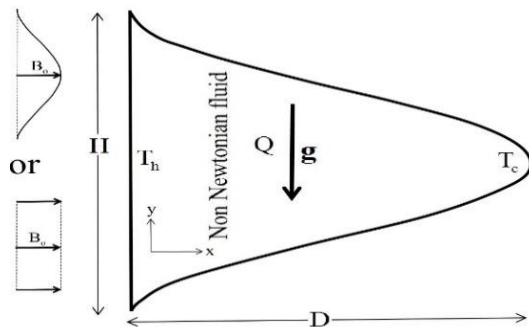


Figure 1. Schematic figure of the present study

3. Equations and numerical model

In order to present the results and analyze the problem, the dimensionless parameters used are presented in equation (3).

$$\begin{aligned} X = \frac{x}{H}, Y = \frac{y}{H}, \quad U = \frac{uH}{\left(\frac{\alpha}{L}\right) Ra^{0.5}}, \\ V = \frac{vH}{\left(\frac{\alpha}{L}\right) Ra^{0.5}}, \quad \theta = \frac{T - T_c}{T_h - T_c}, \\ Ha = BH \sqrt{\frac{\sigma}{\mu_a}}, \quad Ra = \frac{\rho\beta g(T_h - T_c)H^3}{\mu_a\alpha}, \tag{3} \\ Pr = \frac{\mu_a}{\rho\alpha}, \quad \alpha = \frac{k}{\rho C_p}, \\ P = \frac{p}{\rho \left(\frac{\alpha}{H}\right)^2 Ra}, \quad q = \frac{QH^2}{\rho C_p\alpha} \end{aligned}$$

The governing equations used are in the form of Equations (4) – (7) [29].

$$\frac{\partial U}{\partial X} + \frac{\partial V}{\partial Y} = 0 \tag{4}$$

$$\begin{aligned} U \frac{\partial U}{\partial X} + V \frac{\partial U}{\partial Y} = -\frac{\partial P}{\partial X} + \frac{Pr}{\sqrt{Ra}} \left(\frac{\partial \tau_{XX}}{\partial X} + \frac{\partial \tau_{XY}}{\partial Y} \right) \\ - \frac{PrHa^2}{\sqrt{Ra}} U \end{aligned} \tag{5}$$

$$\begin{aligned} U \frac{\partial V}{\partial X} + V \frac{\partial V}{\partial Y} = -\frac{1}{\rho} \frac{\partial P}{\partial Y} + \frac{Pr}{\sqrt{Ra}} \left(\frac{\partial \tau_{XX}}{\partial X} + \frac{\partial \tau_{XY}}{\partial Y} \right) \\ + Pr\theta \end{aligned} \tag{6}$$

$$U \frac{\partial \theta}{\partial X} + V \frac{\partial \theta}{\partial Y} = \frac{1}{\sqrt{Ra}} \left(\frac{\partial^2 \theta}{\partial X^2} + \frac{\partial^2 \theta}{\partial Y^2} \right) + q \tag{7}$$

The stress tensor for a power law non-Newtonian fluid is in the form of relation (8) [36].

$$\tau_{ij} = \mu_a \left(\frac{\partial U_i}{\partial X_j} + \frac{\partial V_j}{\partial Y_i} \right) \tag{8}$$

where μ_a is the apparent viscosity of the non-Newtonian fluid which is given as [37]:

$$\begin{aligned} \mu_a = \\ K \left\{ 2 \left[\left(\frac{\partial U}{\partial X} \right)^2 + \left(\frac{\partial V}{\partial Y} \right)^2 \right] + \left(\frac{\partial U}{\partial X} + \frac{\partial V}{\partial Y} \right)^2 \right\}^{\frac{(n-1)}{2}} \end{aligned} \tag{9}$$

where n and K are the index of power-law model and consistency, respectively. $n=1$, $n<1$ and $n>1$ represent Newtonian fluid, shear thinning fluids and shear thickening fluids respectively.

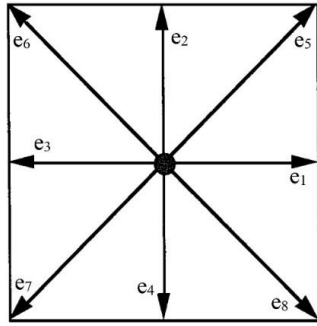


Figure 2. Lattice arrangement for D₂Q₉

In this study, the lattice Boltzmann method is used for simulation. For both flow and temperature field the D₂Q₉ lattice arrangement is used and figure 2 shows a view of this type of lattice. Two distribution functions f_i and h_i are used to calculate the flow field density and the temperature field respectively.

The details and form of this grid arrangement and its advantages are mentioned in various references [38-40]. The algorithm of solving problem in lattice Boltzmann method is shown in figure 3. The macroscopic quantities are obtained as follows [36-38]:

$$T(x, t) = \sum_{i=0}^8 h_i(x, t) \tag{10}$$

$$\rho(x, t) = \sum_{i=0}^8 f_i(x, t) \tag{11}$$

$$\rho u(x, t) = \sum_{i=0}^8 f_i(x, t) e_i \tag{12}$$

The evolution equations are [38-40]:

$$f_i(x + e_i, t + 1) = f_i(x, t) - \frac{[f_i(x, t) - f_i^{eq}(x, t)]}{\tau_1} + F_i \tag{13}$$

$$F_i = 3\rho\omega_i \left[\beta g(T - 0.5) - \frac{Ha^2 \mu_a}{H^2} v \right] \tag{14}$$

$$h_i(x + e_i, t + 1) = h_i(x, t) - \frac{[h_i(x, t) - h_i^{eq}(x, t)]}{\tau_2} + \frac{Q}{\rho C_p} (T - T_c) \tag{15}$$

where F_i is the effect of buoyancy and magnetic force in the form of a source term in Eqs. (13).

The equilibrium distribution functions are given as below:

$$f_i^{eq} = \omega_i \left(1 + 3e_i \cdot u + \frac{9}{2}(e_i \cdot u)^2 - \frac{3}{2}u \cdot u \right) \tag{16}$$

$$h_i^{eq} = \omega_i T (1 + 3e_i \cdot u) \tag{17}$$

The local relaxation time τ can be calculated as below:

$$\eta = \frac{\rho}{3}(\tau_1 - 0.5), \alpha = \frac{\rho}{3}(\tau_2 - 0.5) \tag{18}$$

where τ_1 and τ_2 are independent relaxation parameters for flow and temperature field respectively. The power-law rheological model defined by the equations (19) is a generalization of the Newtonian model, and describe with more accuracy the variation of viscosity η with shear rate γ than the other rheological model and used to shear thinning and shear thickening fluids.

$$\eta = \eta_0 \gamma^{(n-1)} = \eta_0 (S_{\alpha\beta} S_{\alpha\beta})^{(n-1)/2} \tag{19}$$

$S_{\alpha\beta}$ can be calculated locally at each node in the LBM as below:

$$S_{\alpha\beta} = -\frac{3}{2\rho\tau_1} \sum_{i=0}^8 f_i^{(1)} e_{i\alpha} e_{i\beta} \tag{20}$$

where $f_i^{(1)}$ terms are calculated from the non-equilibrium part of the distribution function which is usually measured during collision and τ can be calculated from the local viscosity.

In the presented relations, e represents the microscopic velocity distribution of particles in the lattice directions and is presented in Equation (21) [38-40].

$$e_0 = 0$$

$$e_i = \left[\cos\left(\frac{(i-1)\pi}{2}\right) \cdot \sin\left(\frac{(i-1)\pi}{2}\right) \right]$$

for $i = 1 - 4$

$$e_i = \sqrt{2} \cdot \left[\cos\left(\frac{(i-5)\pi}{2} + \frac{\pi}{4}\right) \cdot \sin\left(\frac{(i-5)\pi}{2} + \frac{\pi}{4}\right) \right]$$

for $i = 5 - 8$

The weighting factors is presented in Equation (22).

$$\omega_0 = \frac{4}{9}$$

$$\omega_i = \frac{1}{9} \quad \text{for } i = 1 - 4$$

$$\omega_i = \frac{1}{36} \quad \text{for } i = 5 - 8$$

The bounce back model has been used to model the smooth walls [40]. For example, for the left vertical wall of the cavity, for the boundary conditions of velocity and temperature are defined as equations (23) and (24).

$$f_1 = f_3 \cdot f_5 = f_8 \cdot f_8 = f_6 \tag{23}$$

$$h_1 = T_h(\omega_1 + \omega_3) - h_3$$

$$h_5 = T_h(\omega_5 + \omega_7) - h_7 \tag{24}$$

$$h_8 = T_h(\omega_8 + \omega_6) - h_6$$

To calculate the velocity and temperature on curved boundaries, methods applied by Nemati et al. [39] have been used. Figure 4 shows the curved boundary and their grid arrangement. In this method, out of the nodes in the solid boundary area, only nodes enter the computational domain adjacent to the curved boundary. These nodes are marked with the subtitle b. The intersection of the network's eighty directions with the curved boundary with the subtitle w is shown. The first and second nodes in each of the mentioned directions within the computational area are also denoted by the subtitles f and ff, respectively. In this method, after the collision step, the density and energy distribution functions for the nodes adjacent to the boundary within the domain are calculated using the extrapolation and with the temperature conditions and curve boundary velocity. For the streaming step, the calculated distribution functions in the solid boundary nodes are transferred to the nodes within the solution domain. The extrapolation will be from the first or second order, depending on the intersection of the curved boundary and the grid network directions. For this purpose, the parameter Δ is defined in the form $\Delta = |x_f - x_w|/|x_f - x_b|$ to be used to calculate density and energy distribution functions.

To have a measure of the amount of heat transfer, the average Nusselt number is given locally and average on the hot wall of the enclosure in Equations (25) and (26).

It should also be noted that the convergence criterion in the present work is considered as equation (27) that b and b+1 represent the old and new time phases and N and M represent the number of nodes in the x and y directions, respectively. The parameter Γ stands for U, V or θ .

$$Nu_Y = \frac{Q_{convection}}{Q_{conduction}} = -\left(\frac{\partial\theta}{\partial X}\right)_{X=0} \tag{25}$$

$$Nu = \frac{1}{H} \int_0^1 -\left(\frac{\partial\theta}{\partial X}\right)_{X=0} dY \tag{26}$$

$$\chi = \frac{\sum_{i=1}^N \sum_{j=1}^M |\Gamma^{b+1} - \Gamma^b|}{\sum_{i=1}^N \sum_{j=1}^M |\Gamma^b|} \leq 10^{-6} \tag{27}$$

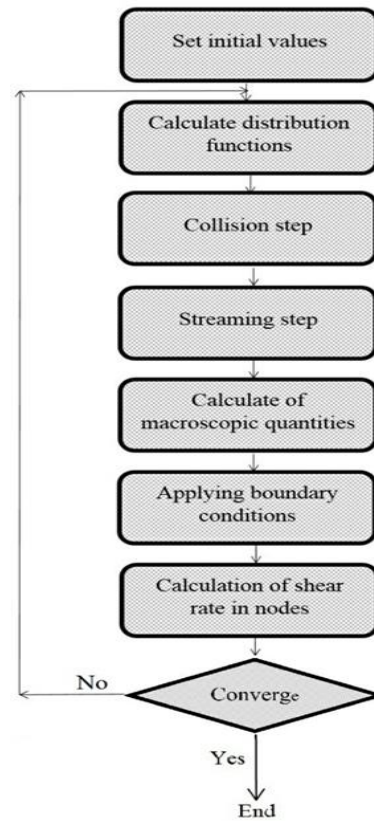


Figure 3. Algorithm of the LBM

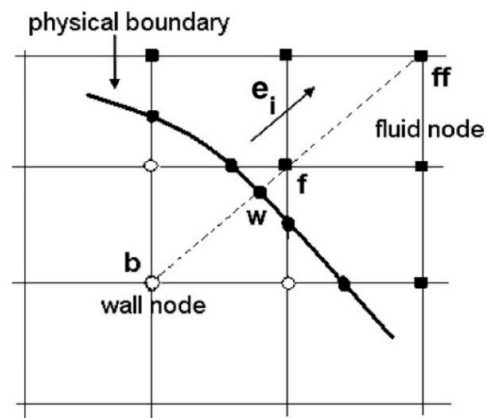


Figure 4. The boundary of the curved wall and the nodes

4. Grid independence study and validations

In order to find a suitable mesh grid that leads to the independence of the results from the enclosure mesh size, the Nusselt number on average on the vertical and hot wall of the enclosure and maximum value of streamlines (shown in table with MVS) in two non-Newtonian power index ($n=0.8, 1.2$) for different grid sizes has been obtained and provided in table 1. Also figure 5 shows the horizontal velocity for different values of mesh size. According to table 1 and figure 5, it was observed that by selecting mesh size 100×100 , it is possible to ensure that the results are not as dependent as the computational network.

In order to validate the written code, the present work is compared with the reference [29] for $Ra=10^5$ and $Ha=20$ in figure 6. The natural convection of a power law non newtonian fluid in a C-shaped cavity which were numerically investigated. In order to check the numerical method and ensure the performance of natural convection heat transfer simulation by the present code under the influence of a magnetic field, the present numerical code has been validated with the published study of reference [41] for the same cavity which is given in table 2 for $Ra=10^5$. Also, to verify the code written in the face of the curved boundary, the present work is compared with the reference [42] and presented in figure 7. As can be seen, the results of the present work show an acceptable consistency and the correctness of the written code can be ensured.

5. Results and discussion

Due to the validation of the computer program and ensuring the accuracy of the results, the results of the simulations are presented and expressed in this section.

According to figure 8 that shows the effect of increasing the power index and magnetic field strength on isotherms. It is observed that in all values of Hartmann number, with increasing power index, due to increasing the apparent viscosity of the fluid, the scattering of isothermal lines inside the enclosure decreases significantly. Increasing the power index reduces the curvature of the lines, which indicates a decrease in convection within the enclosure. The parallelism of isothermal lines at $n=1.2$ indicates the predominance of thermal conductivity.

At all values of the power index, with increasing Hartmann number, the curvature of the lines decreases and the convection effects decrease. Because in this case the Lorentz force, the resistive force of the fluid flow, increases and leads to a decrease in flow velocity. This effect decreases with increasing power index. Because in this case, the effects of thermal conductivity are dominant. The decrease in fluid velocity with increasing power index and Hartmann number is clearly shown in figure 9. It can be seen that the effect of the magnetic field decreases significantly with increasing power index. It is observed that increasing the power index from 0.8 to 1.2 caused reduces the maximum velocity about 85%. According to figure 10, it can be seen that increasing the Hartmann number reduces the curvature of the temperature profile, which indicates that the thermal conductivity dominant over the convection, and this effect is very small at $n=1.2$. Because in the case of a shear thickening fluids, the conduction is the dominant heat transfer phenomenon and the effect of the magnetic field is negligible. Figure 11 shows that As the Hartmann number and fluid power index increase, the average Nusselt number decreases. The effect of increasing the Hartmann number on reducing the average Nusselt number in the shear thinning fluid state is

greatest. Because in this case, convection has the highest effect on heat transfer. Increasing the Hartmann number from zero to 60, decreases the average Nusselt number by 21, 15, and 3 percent for shear thinning fluid, Newtonian fluid, and shear thickening fluid respectively. Figure 12 shows the effect of the type of magnetic field applied on streamlines and isotherms. In all cases, the fluid heats up near the vertical wall and moves upwards, and after colliding with the cold wall, moves downwards, causing clockwise vortices inside the enclosure.

It can be seen that the non-uniform applied of the magnetic field in addition to changes the shape of the streamlines, the strength of the vorticities also changes. When a non-uniform magnetic field is applied, the Lorentz force gradient decreases along the vertical axis, which increases the protection strength inside the enclosure. The strength of the vortex formed at $\kappa=2$ is about twice that of a uniform applied magnetic field. Applying periodic magnetic field also causes the isothermal lines to become wavy, which causes the lines to be compressed in some areas, which increases the average Nusselt number.

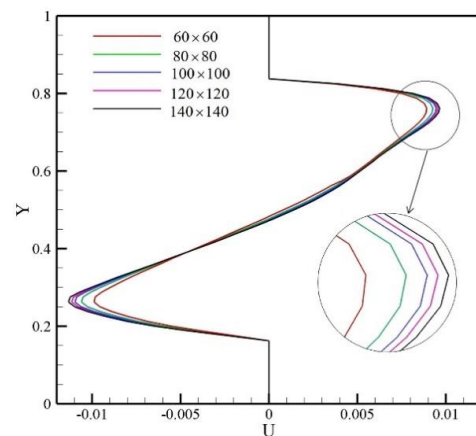


Figure 5. Effect of number of mesh size on the horizontal velocity at $Ha=30$, $\kappa=1$, $q=0$, $n=0.8$

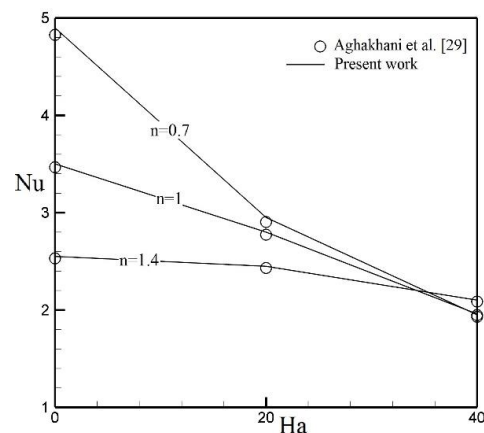


Figure 6. Comparison of the average Nusselt numbers of present code against Aghakhani et al. [29]

Table 1. Average Nusselt number and maximum value of streamlines (MVS) at AR=1, Ha=30, $\kappa=1$ and $q=0$.

n	Mesh size	60×60	80×80	100×100	120×120	140×140
n=0.8	Nu	13.825	14.345	14.683	14.852	14.865
	Error (%)	-	3.764	2.325	1.151	0.085
	MVS	0.144	0.153	0.161	0.163	0.163
n=1.2	Nu	13.601	13.883	14.059	14.061	14.061
	Error (%)	-	2.073	1.267	0.015	0
	MVS	0.012	0.013	0.014	0.014	0.014

Table 2. Comparison of the average Nusselt numbers between the present work and Sathiyamoorthy and Chamkha [41] at Ra=10⁵

Ha	Present work	Sathiyamoorthy and Chamkha [41]	Percentage of difference
0	13.051	13.182	0.98
50	12.489	12.75	2.04
100	11.919	12.23	2.55

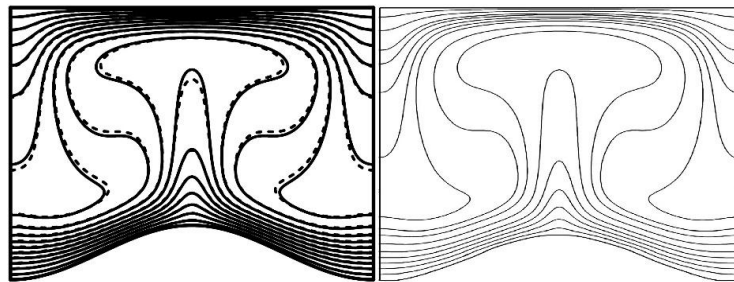


Figure 7. Comparison of isothermal lines for Ra=105 between numerical study by Shahriari and ashorynejad [42] (Left) and the present work (Right)

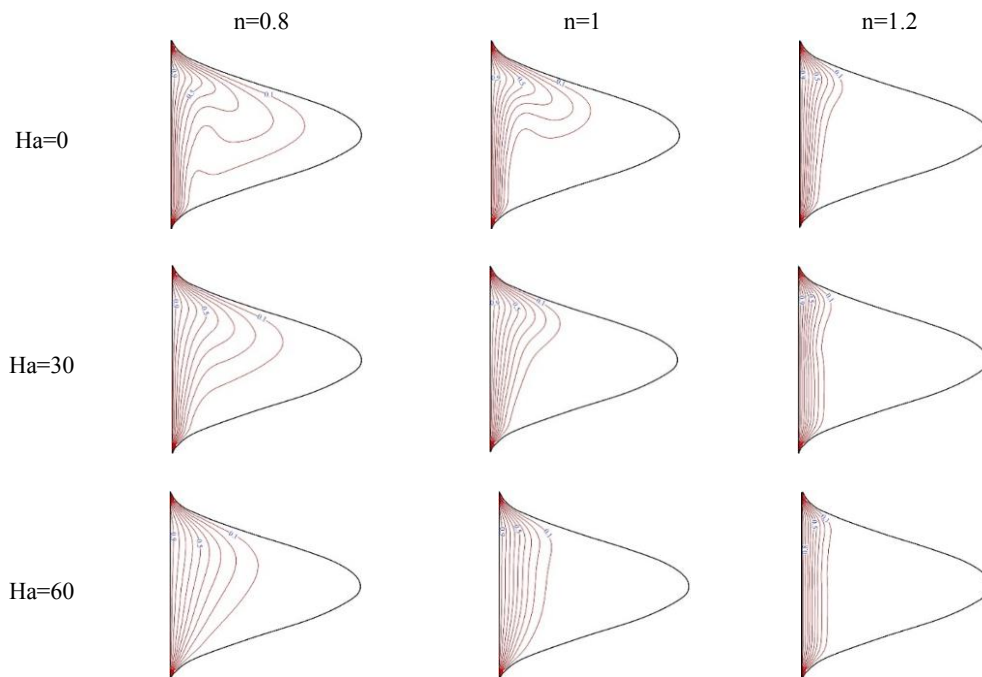


Figure 8. Isotherms for various power law indexes and Hartmann numbers at AR=1, $\kappa=1$ and $q=0$

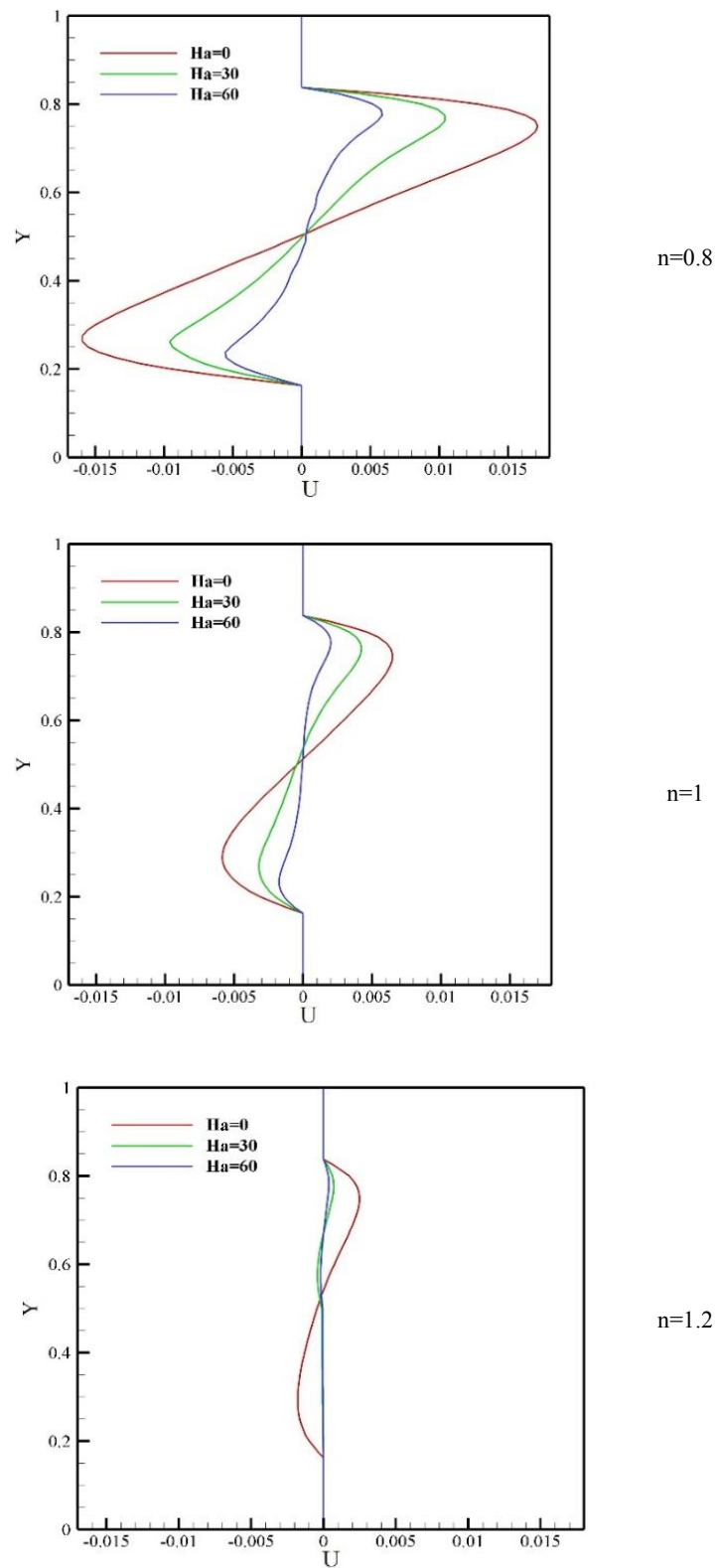


Figure 9. Horizontal velocity in $X=0.25$ for various power law indexes and Hartmann numbers at $AR=1$, $\kappa=1$ and $q=0$

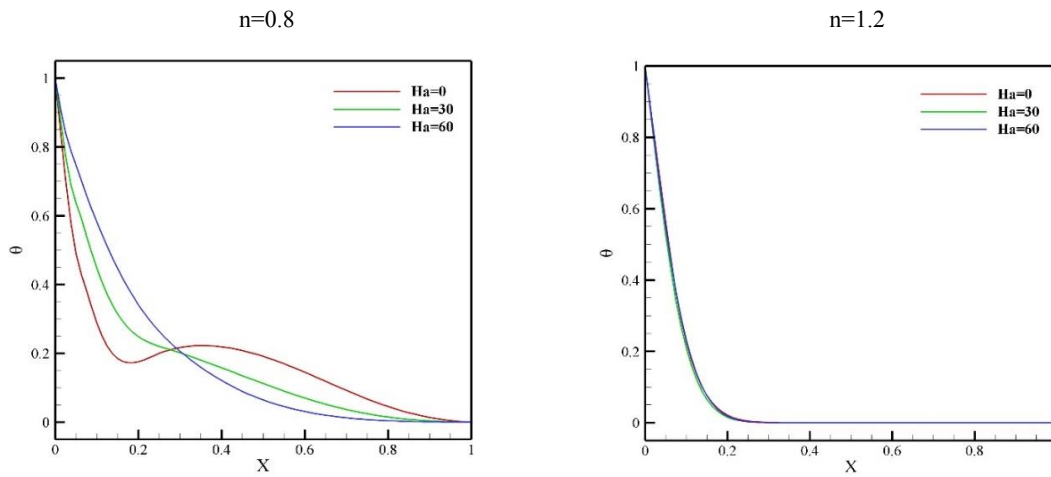


Figure 10. Dimensionless temperature in $Y=0.5$ for various power law indexes and Hartmann numbers at $AR=1$, $\kappa=1$ and $q=0$

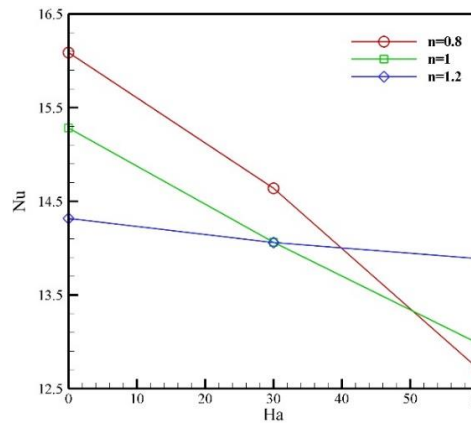


Figure 11. Average Nusselt numbers for various power law indexes and Hartmann number at $AR=1$, $\kappa=1$ and $q=0$

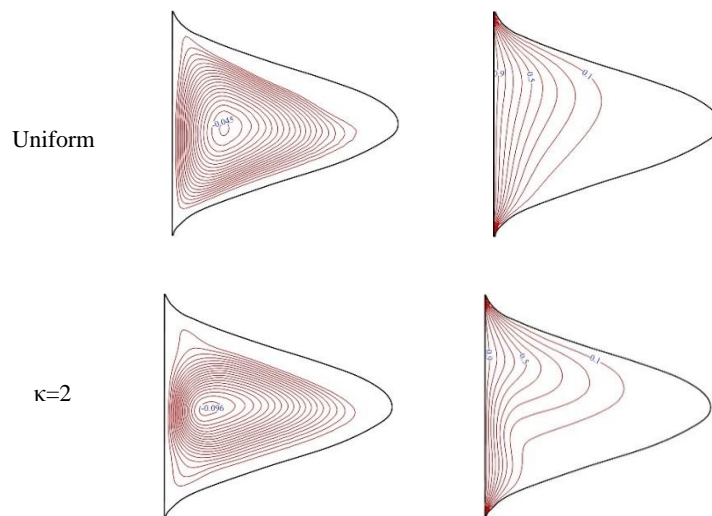


Figure 12. Streamlines and isotherms for uniform magnetic and periodic ($\kappa=2$) magnetic field at $AR=1$, $n=1$ and $q=0$

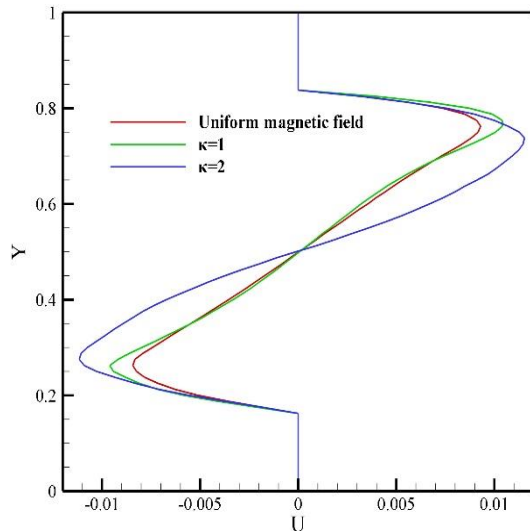


Figure 13. Horizontal velocity in $X=0.25$ for various types of magnetic field applied at $AR=1$, $Ha=30$ and $q=0$

According to figure 13, the velocity of the fluid inside the enclosure is a function of the type of magnetic field applied and the maximum velocity is related to the two oscillating waves of the magnetic field. Applying a magnetic field with two oscillating waves caused increases 38% of the maximum velocity.

According to table 3, the periodic magnetic field will have a higher Nusselt number compared to the uniform which this effect is negligible for the shear thickening fluid.

Figure 14 shows streamlines and isotherms for different values of power index and heat absorption/generation coefficient. According to the figure 14, in all values of the power index, with increasing q , the flow strength inside the enclosure increases and for $n=1.2$ a single vortex is broken into two vortices.

A stronger vortex forms vicinity the hot wall while a weaker vortex forms near the cold wall. In the case of heat absorption ($q=-10$), because the temperature of the fluid is much lower than the wall, the isothermal lines are not wide in the enclosure and are dense in the vicinity of the hot wall. However, in the case of heat generation ($q=+10$), the scattering of isotherms in the enclosure increases and as the temperature of the fluid inside the enclosure increases, the density of isotherms near the hot wall decreases, which reduces the Nusselt number.

This effect is more obvious in the case of shear thinning

fluid and insignificant for shear thickening fluid. The highest temperature of the fluid inside the enclosure is seen in the heat generation mode and for the shear thinning fluid.

According to figure 15, with increasing the heat absorption/generation coefficient, the temperature of the fluid in the enclosure increases and this effect decreases with increasing the power index, and this effect is negligible in the shear thickening fluid. Because in this case, conduction heat transfer is dominant.

Figure 16 shows that in all values of the power index, increasing the heat absorption/generation coefficient reduces the average Nusselt number, which for shear thinning fluid, Newtonian fluid and shear thickening fluid is about 74, 45 and 28 percent, respectively. Because increasing the power index increases the apparent viscosity and leads to the dominant of thermal conductivity.

Figure 17 shows that with increasing the power index, strength of the fluid flow inside the enclosure decrease because of the apparent viscosity increases which this effect increases with increasing the aspect ratio of the enclosure. Because with increasing the aspect ratio, the moving space of the fluid increases and the convection power increases.

Increasing the flow flow strength by reducing the apparent viscosity causes the flow lines to stretch along the enclosure and cover a larger area of the enclosure. At $AR=0.5$, due to the small moving space of the fluid flow, in the shear thickening fluid state, a low-strength secondary vortex does not form inside the enclosure. For $AR=1.5$, a counterclockwise secondary vortex is formed near the cold wall. It is also observed that the effect of increasing the power index on isothermal lines is more obvious for the aspect ratio of 1.5.

According to table 4, increasing the Hartmann number leads to a decrease in maximum flow lines, which increases with increasing the aspect ratio of the enclosure. According to the table 4, it can be seen that increasing the power index from 0.8 to 1.2 causes a decrease of 93, 84 and 61 percent of the maximum flow lines for Hartmann numbers 0, 30 and 60, respectively. Because with increasing the power index increases the apparent viscosity and reduces the velocity of the fluid. The negative values in the table indicate that the vortices formed are clockwise.

Table 3. Average nusselt numbers for various types of magnetic field applied, Hartmann numbers and power law indexes at AR=1and q=0

	n=0.8			n=1			n=1.2		
	Uniform	$\kappa=1$	$\kappa=2$	Uniform	$\kappa=1$	$\kappa=2$	Uniform	$\kappa=1$	$\kappa=2$
Ha=30	14.052	14.638	15.457	13.709	14.061	14.874	14.001	14.059	14.101
Ha=60	12.262	12.709	13.304	12.721	12.981	13.438	13.885	13.887	13.887

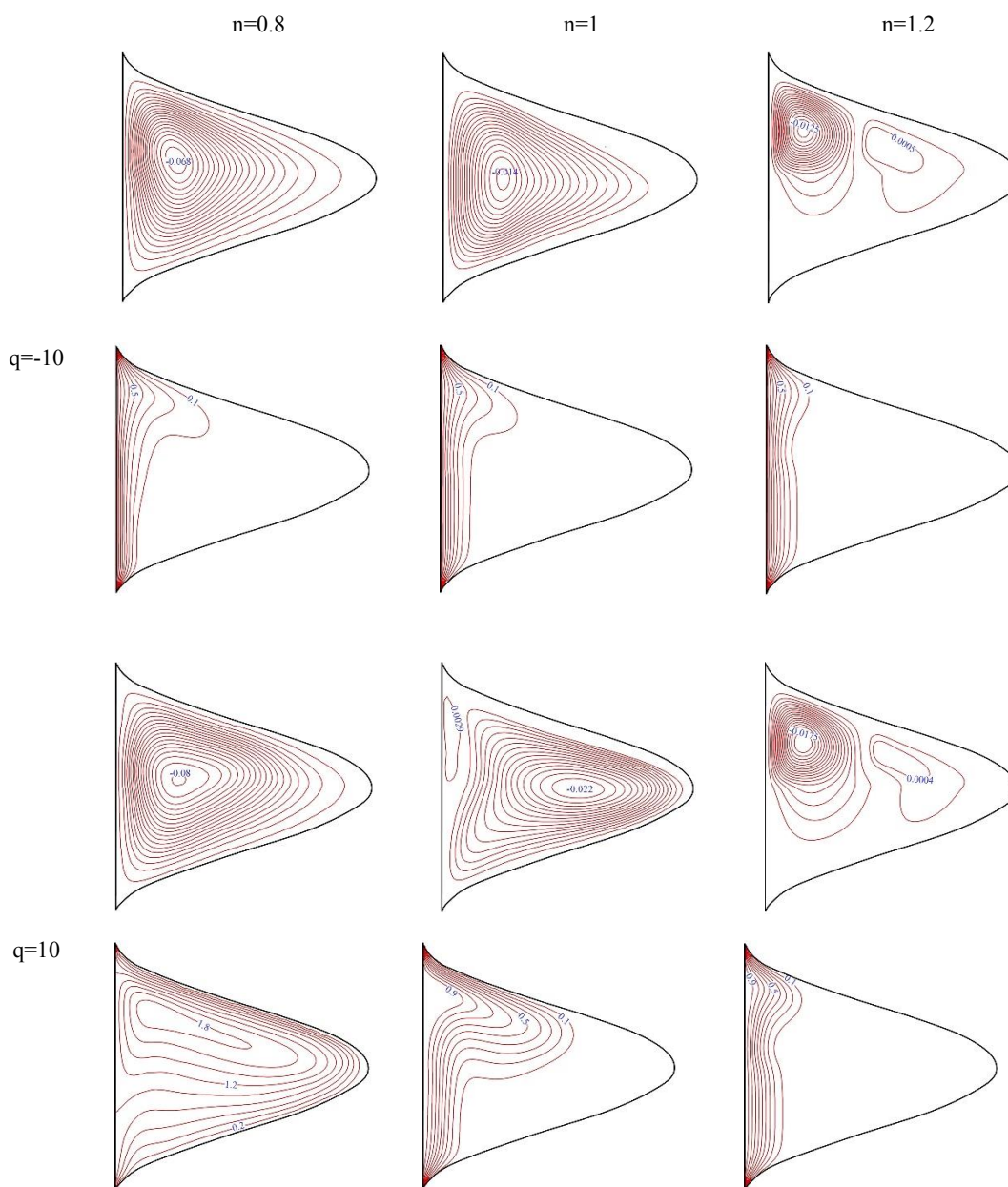


Figure 14. Streamlines and isotherms for various power law indexes and heat absorption/generation coefficient at Ha=0 and AR=1

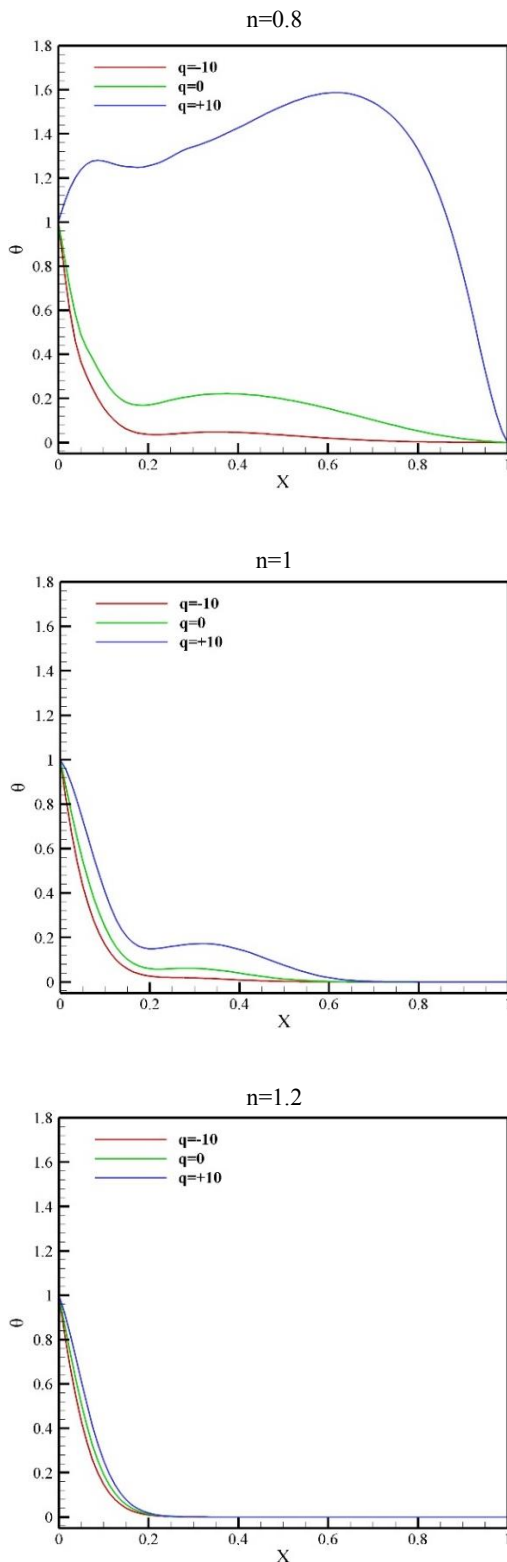


Figure 15. Dimensionless temperature in $Y=0.5$ for various heat absorption/generation coefficient and power law indexes at $Ha=0$ and $AR=1$

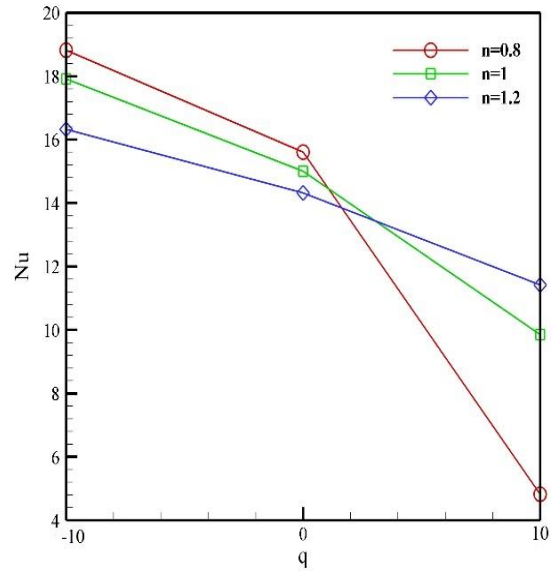


Figure 16. Average Nusselt numbers for various power law indexes and heat absorption/generation coefficient at $Ha=0$ and $AR=1$

According to table 4, increasing the Hartmann number leads to a decrease in maximum flow lines, which increases with increasing the aspect ratio of the enclosure.

According to the table 4, it can be seen that increasing the power index from 0.8 to 1.2 causes a decrease of 93, 84 and 61 percent of the maximum flow lines for Hartmann numbers 0, 30 and 60, respectively. Because with increasing the power index increases the apparent viscosity and reduces the velocity of the fluid. The negative values in the table indicate that the vortices formed are clockwise.

According to figure 18, increasing the Hartmann number in all three aspect ratios reduces the average Nusselt number, and this effect increases with increasing aspect ratio. Because with increasing the aspect ratio, the motion space of the fluid and the convection effects increase, which can be obtained by comparing the slope of the diagrams.

According to table 18 in all values of the Hartmann number, decreasing the aspect ratio increases the average Nusselt number. Because by reducing the aspect ratio, the cold walls of the enclosure become closer to the hot wall and the rate of heat transfer increases.

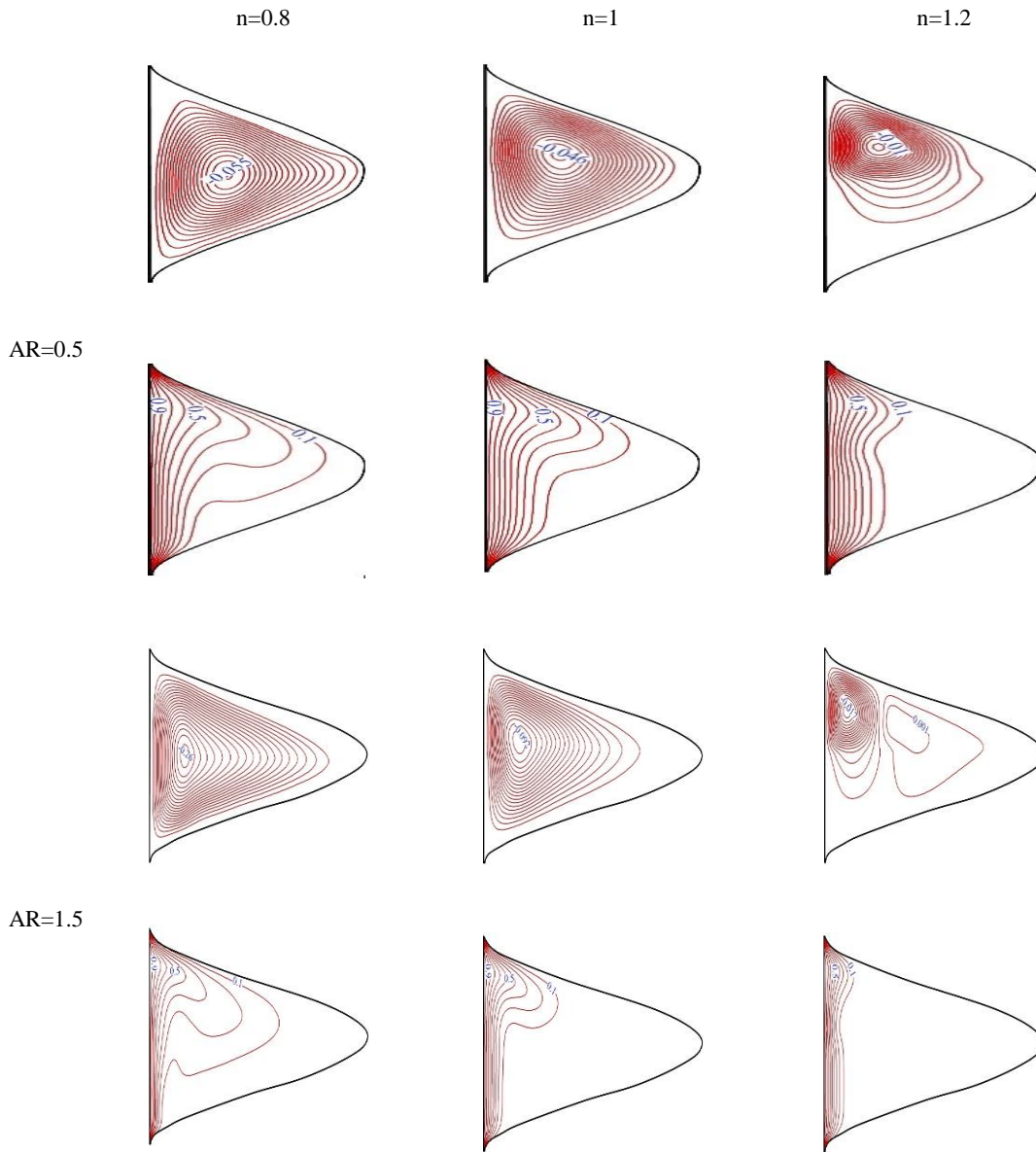


Figure 17. Streamlines and isotherms for various power law indexes and aspect ratio at $Ha=0$ and $q=0$

Table 4. Maximum value of streamlines (MVS) for various Hartmann numbers, power law indexes and aspect ratio at $\kappa=0$ and $q=0$

	n=0.8			n=1			n=1.2		
	AR=0.5	AR=1	AR=1.5	AR=0.5	AR=1	AR=1.5	AR=0.5	AR=1	AR=1.5
Ha=0	-0.055	-0.211	-0.262	-0.046	-0.084	-0.092	-0.011	-0.015	-0.017
Ha=30	-0.044	-0.148	-0.163	-0.037	-0.063	-0.068	-0.009	-0.014	-0.015
Ha=60	-0.031	-0.085	-0.076	-0.029	-0.041	-0.034	-0.009	-0.013	-0.014

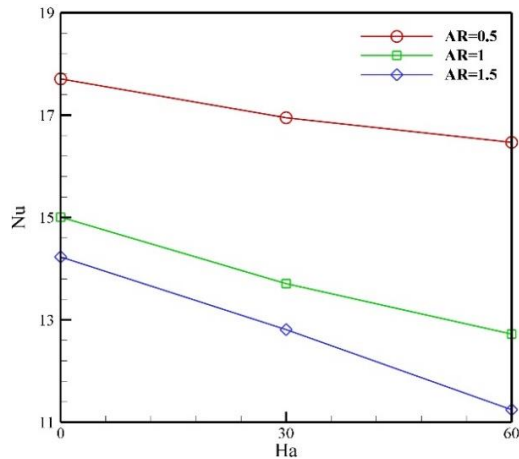


Figure 18. Average Nusselt numbers for various Hartmann numbers and aspect ratio at $n=1$ and $q=0$ in uniform magnetic field

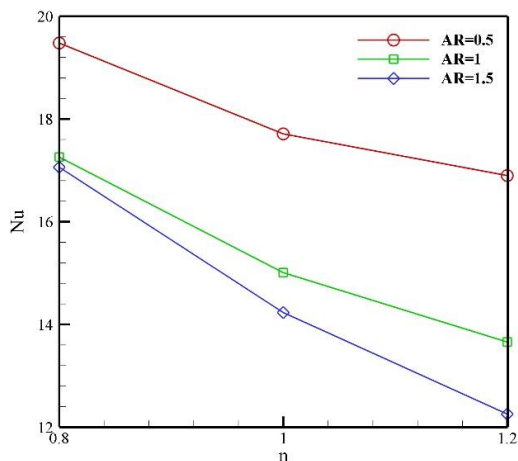


Figure 19. Average nusselt numbers for various Hartmann numbers and aspect ratio at $Ha=0$ and $q=0$

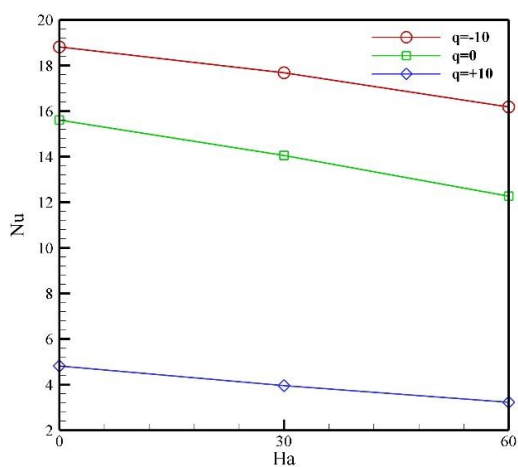


Figure 20. Average nusselt numbers for various heat absorption/generation coefficient and Hartmann numbers at $n=0.8$ and $AR=1$ in uniform magnetic field

Figure 19 shows that the effect of increasing the power index on reducing the average Nusselt number increases with increasing the aspect ratio of the enclosure. By increasing the power index from 8 to 12, the average Nusselt number decreases by about 23, 33 and 44% for the aspect ratio of 5, 1 and 15, respectively. According to figure 20, with increasing Hartmann number, the effect of decreasing the average Nusselt number increases with increasing heat absorption /generation coefficient. Because in this case, both factors reduce amount of heat transfer (magnetic field and heat generation). Because these two parameters strengthen each other in further reducing the rate of heat transfer.

Conclusions

In the present study, the effect of magnetic field and heat absorption/generation coefficient on the natural convection of non-Newtonian fluid in a two dimensional enclosure with variable aspect ratio is investigated by the lattice Boltzmann method. The simulation was performed by writing computer code in Fortran language. The results were compared and validated with previous studies and the accuracy of the results was ensured. The effect of Hartmann number, heat absorption/ generation coefficient, non-Newtonian power index, aspect ratio of the enclosure and type of magnetic field applied is investigated. The most important results can be summarized as follows:

- 1- Increasing the Hartmann number reduces the power of fluid flow in the enclosure and the heat transfer due to reduce velocity. This effect decreases with increasing power index and decreasing the aspect ratio of the enclosure. On average, increasing the Hartmann number from zero to 60 reduces the average Nusselt number by about 20%.
- 2- Increasing the power index due to increasing the apparent viscosity of the fluid reduces the average Nusselt number and flow strength, which increases with increasing the aspect ratio of the enclosure and heat absorption/generation coefficient.
- 3- Increasing the aspect ratio of the enclosure increases the flow strength by about 45% and decreases the average Nusselt number by about 25%.
- 4- Periodically applying a magnetic field increase the flow strength by 40% and the average Nusselt number by about 10%. The effect of applying the periodic magnetic field, decreases with increasing power index.
- 5- Increasing heat absorption/generation coefficient reduces the average Nusselt number and increases the flow power. Simultaneous increase in the Hartmann number and heat absorption/generation coefficient results in a lower average Nusselt number.

Nomenclature

AR	Aspect ratio
B	Magnetic field strength
C_p	Heat capacity
D	Length of the enclosure
e_i	Discrete particle speeds
f	Density distribution functions
f^{eq}	Equilibrium density distribution functions
F	External forces
g	Acceleration due to gravity
h	Internal energy distribution functions
h^{eq}	Equilibrium internal energy distribution functions
H	Height of the enclosure
Ha	Hartmann number
n	Non-Newtonian power index
Nu	Nusselt number
P	Pressure
Pr	Prandtl number
q	Heat generation/absorption coefficient
Ra	Rayleigh number
T	Temperature
u(u,v)	Velocities
x(x,y)	Cartesian coordinates
Greek symbols	
α	Thermal diffusivity
κ	Number of oscillating waves
τ	Shear stress
τ_1	Relaxtion time for flow
τ_2	Relaxtion time for temperature
ρ	Density
μ_a	Apparent viscosity
θ	Dimensionless temperature
ω	Weighting factor
Subscripts	
c	Cold
h	Hot
i	Discrete lattice direction

References

- [1] Hetsroni, G., Mosyak, A., Rozenblit, R., Pogrebnyak, E., Segal, Z., 2009. Natural convection boiling of water and surfactant solutions having negligible environmental impact in vertical confined space. *International journal of multiphase flow*, 35(1), pp. 20-33.
- [2] Varol, Y., 2012. Natural convection for hot materials confined within two entrapped porous trapezoidal cavities. *International communications in heat and mass transfer*, 39(2), pp. 282-290.
- [3] Ghoreishi-Madiseh, S. A., Amiri, L., Sasmito, A. P., Hassani, F. P., 2021. A conjugate natural convection model for large scale seasonal thermal energy storage units: application in mine ventilation. *Energy Procedia*, 105, pp. 4167-4172.
- [4] Rallabandi, S. R., 2017. Analytical and numerical investigation of heat and mass transfer effects on magnetohydrodynamic natural convective flow past a vertical porous plate. *Journal of Heat and Mass Transfer Research*. 4(2), pp. 117-133.
- [5] Ahmad, M. M., Imran, M. A., Aleem, M., Khan, I., 2019. A comparative study and analysis of natural convection flow of MHD non-Newtonian fluid in the presence of heat source and first-order chemical reaction. *Journal of Thermal Analysis and Calorimetry*. 137(5), pp. 1783-1796.
- [6] Zhang, R., Ghasemi, A., Barzinjy, A. A., Zareei, M., Hamad, S. M., Afrand, M., 2020. Simulating natural convection and entropy generation of a nanofluid in an inclined enclosure under an angled magnetic field with a circular fin and radiation effect. *Journal of Thermal Analysis and Calorimetry*. 139(6), pp. 3803-3816.
- [7] Yan, S. R., Pordanjani, A. H., Aghakhani, S., Goldanlou, A. S., Afrand, M., 2020. Managment of natural convection of nanofluids inside a square enclosure by different nano powder shapes in presence of Fins with different shapes and magnetic field effect. *Advanced Powder Technology*. 31(7), pp. 2759-77.
- [8] Fleishman, G. D., Anfinogentov, S., Loukitcheva, M., Mysh'yakov, I., Stupishin, A., 2017. Casting the coronal magnetic field reconstruction tools in 3D using the MHD bifrost model. *The Astrophysical Journal*. 839(1), pp. 30-30.
- [9] Wang, H., Xuan, W., Zhang, Z., Qin, B., 2019. Experimental investigation of the properties of dust suppressants after magnetic-field treatment and mechanism exploration. *Powder Technology*. 342, pp. 149-155.
- [10] Farajpour, M. R., Shahidi, A., Farajpour, A., 2018. Resonant frequency tuning of nanobeams by piezoelectric nanowires under thermo-electro-magnetic field: a theoretical study. *Micro & Nano Letters*. 13(11), pp. 1627-1632.
- [11] Lu, S., He, B., Gao, D., Chen, W., Li, X., 2020. Numerical simulation of double-diffusive

- natural convection in an enclosure in the presence of magnetic field with heat-conducting partition using lattice Boltzmann method. *Journal of Thermal Analysis and Calorimetry*. 135(4), pp. 1-8.
- [12] Ma, Y., Mohebbi, R., Rashidi, M. M., Yang, Z., Sheremet, M. A., 2019. Numerical study of MHD nanofluid natural convection in a baffled U-shaped enclosure. *International Journal of Heat and Mass Transfer*. 130, pp. 123-134.
- [13] Hayat, T., Ullah, I., Alsaedi, A., Ahmad, B., 2019. Variable aspects of double stratified MHD flow of second grade nanofluid with heat generation/absorption: A revised model. *Radiation Physics and Chemistry*. 157, pp. 109-115.
- [14] Jami, M., Mezrhab, A., Bouzidi, M. H., Lallemand, P., 2007. Lattice Boltzmann method applied to the laminar natural convection in an enclosure with a heat-generating cylinder conducting body. *International Journal of Thermal Sciences*. 46(1), pp. 38-47.
- [15] Maleki, H., Safaei, M. R., Togun, H., Dahari, M., 2019. Heat transfer and fluid flow of pseudo-plastic nanofluid over a moving permeable plate with viscous dissipation and heat absorption/generation. *Journal of Thermal Analysis and Calorimetry*. 135(3), pp. 1643-1654.
- [16] Selimefendigil, F., Öztop, H. F., 2016. Natural convection in a flexible sided triangular cavity with internal heat generation under the effect of inclined magnetic field. *Journal of Magnetism and Magnetic Materials*. 417, pp. 327-337.
- [17] Mliki, B., Abbassi, M. A., Omri, A., Zeghami, B., 2015. Augmentation of natural convective heat transfer in linearly heated cavity by utilizing nanofluids in the presence of magnetic field and uniform heat generation/absorption. *Powder Technology*. 284, pp. 312-325.
- [18] Yazdani, K., Sahebamei, M., Ahmadpour, A., 2020. Natural convection heat transfer and entropy generation in a porous trapezoidal enclosure saturated with power-law non-Newtonian fluids. *Heat Transfer Engineering*. 41(11), pp. 982-1001.
- [19] Massoudi, M. D., Hamida, M. B., 2020. MHD natural convection and thermal radiation of diamond-water nanofluid around rotating elliptical baffle inside inclined trapezoidal cavity. *The European Physical Journal Plus*. 135(11), pp. 1-24.
- [20] Dhiman, A., Ghosh, R., Baranyi, L., 2019. Hydrodynamic and thermal study of a trapezoidal cylinder placed in shear-thinning and shear-thickening non-Newtonian liquid flows. *International Journal of Mechanical Sciences*. 157, pp. 304-319.
- [21] Li, Z., Shahsavari, A., Niazi, K., Al-Rashed, A. A., Talebizadehsardari, P., 2020. The effects of vertical and horizontal sources on heat transfer and entropy generation in an inclined triangular enclosure filled with non-Newtonian fluid and subjected to magnetic field. *Powder Technology*. 364, pp. 924-942.
- [22] Lukose, L., Biswal, P., Basak, T., 2020. Analysis of flow and thermal maps during natural convection within porous triangular configurations subjected to linear heating at inclined walls. *Numerical Heat Transfer, Part A: Applications*. 78(9), pp. 479-503.
- [23] Dogonchi, A. S., Ganji, D. D., 2015. Investigation of heat transfer for cooling turbine disks with a non-Newtonian fluid flow using DRA. *Case Studies in Thermal Engineering*. 6, pp. 40-51.
- [24] Aldi, N., Buratto, C., Casari, N., Dainese, D., Mazzanti, V., Mollica, F., Munari, E., Occari, M., Pinelli, M., Randi, S., Spina, P. R., 2017. Experimental and Numerical Analysis of a non-Newtonian Fluids processing pump. *Energy Procedia*. 126, pp. 762-769.
- [25] Lare, A. I., 2015. Casson fluid flow with variable viscosity and thermal conductivity along exponentially stretching sheet embedded in a thermally stratified medium with exponentially heat generation. *Journal of Heat and Mass Transfer Research*. 2(2), pp. 63-78.
- [26] Adam, S., Premnath, K. N., 2019. Numerical investigation of the cascaded central moment lattice Boltzmann method for non-Newtonian fluid flows. *Journal of Non-Newtonian Fluid Mechanics*. 274, pp. 104188.
- [27] Qi, Z., Kuang, S., Yu, A., 2019. Lattice Boltzmann investigation of non-Newtonian fluid flow through a packed bed of uniform spheres. *Powder Technology*. 343, pp. 225-236.
- [28] Raisi, A., 2015. The influence of a pair constant temperature baffles on power-law fluids natural convection in a square enclosure. *Modares Mechanical Engineering*. 15(11), pp. 215-224.
- [29] Aghakhani, S., Pordanjani, A. H., Karimipour, A., Abdollahi, A., Afrand, M., 2018. Numerical investigation of heat transfer in a power-law non-Newtonian fluid in a C-Shaped cavity with magnetic field effect using finite difference lattice Boltzmann method. *Computers & Fluids*. 176, pp. 51-67.

- [30] Alpak, F. O., Zacharoudiou, I., Berg, S., Dietderich, J., Saxena, N., 2019. Direct simulation of pore-scale two-phase visco-capillary flow on large digital rock images using a phase-field lattice Boltzmann method on general-purpose graphics processing units. *Computational Geosciences*. 23(5), pp. 849-880.
- [31] Sajjadi, H., Delouei, A. A., Izadi, M., Mohebbi, R., 2019. Investigation of MHD natural convection in a porous media by double MRT lattice Boltzmann method utilizing MWCNT-Fe3O4/water hybrid nanofluid. *International Journal of Heat and Mass Transfer*. 132, pp. 1087-1104.
- [32] Mohammadian, S. K., Zhang, Y., 2019. Convection heat transfer with internal heat generation in porous media: Implementation of thermal lattice Boltzmann method. *Numerical Heat Transfer, Part A: Applications*. 76(3), pp. 101-114.
- [33] Zhang, R., Aghakhani, S., Pordanjani, A. H., Vahedi, S. M., Shahsavar, S. M., Afrand, M., 2020. Investigation of the entropy generation during natural convection of Newtonian and non-Newtonian fluids inside the L-shaped cavity subjected to magnetic field: application of lattice Boltzmann method, *The European Physical Journal Plus*, 135, pp. 184-201.
- [34] Mehryan, S. A., Izadi, M., Chamkha, A. J., Sheremet, M. A., 2018. Natural convection and entropy generation of a ferrofluid in a square enclosure under the effect of a horizontal periodic magnetic field. *Journal of Molecular Liquids*. 263, pp. 510-525.
- [35] Izadi, M., Sheremet, M. A., Mehryan, S. A., 2020. Natural convection of a hybrid nanofluid affected by an inclined periodic magnetic field within a porous medium. *Chinese Journal of Physics*. 263, pp. 410-4255.
- [36] Kefayati, G. R., 2015. Mesoscopic simulation of magnetic field effect on natural convection of power-law fluids in a partially heated cavity. *Chemical Engineering Research and Design*. 94, pp. 337-354.
- [37] Kefayati, G. R., Tang, H., Chan, A., Wang, X., 2018. A lattice Boltzmann model for thermal non-Newtonian fluid flows through porous media. *Computers & Fluids*. 176, pp. 226-244.
- [38] Kefayati, G. R., Gorji-Bandpy, M., Sajjadi, H., Ganji, D. D., 2012. Lattice Boltzmann simulation of MHD mixed convection in a lid-driven square cavity with linearly heated wall. *Scientia Iranica*. 19(4), pp. 1053-1065.
- [39] Nemati, M., Sefid, M., Rahmati, A. R., 2020. The effect of changing the position of the hot wall and increasing the amplitude and number of oscillations of wavy wall on the flow and heat transfer of nanofluid inside the channel in the presence of magnetic field. *Journal of solid and fluid Mechanics*. 10, pp. 219-236.
- [40] Nemati, M., Rahmati, A. R., 2018. Investigation of Magnetic Field Effect on Nanofluid Mixed Convection inside Lid-Driven K-shaped Enclosure Using Lattice Boltzmann Method. *Journal of solid and fluid Mechanics*. 8, pp. 111-126.
- [41] Sathiyamoorthy, M., Chamkha, A., 2010. Effect of magnetic field on natural convection flow in a liquid gallium filled square cavity for linearly heated side wall (s). *International Journal of Thermal Sciences*. 49(9), pp. 1856-1865.
- [42] Shahriari, A., Ashorynejad, H. R., 2017. Numerical study of heat transfer and entropy generation of Rayleigh-Benard convection nanofluid in wavy cavity with magnetic field. *Modares Mechanical Engineering*. 17(10), pp. 385-396.